

# A numerical simulation of high efficiency CdS/CdTe based solar cell using NiO HTL and ZnO TCO



Shamim Ahmmmed <sup>a,b</sup>, Asma Aktar <sup>a</sup>, Md. Ferdous Rahman <sup>a,c</sup>, Jaker Hossain <sup>a</sup>, Abu Bakar Md. Ismail <sup>a,\*</sup>

<sup>a</sup> Solar Energy Laboratory, Department of Electrical and Electronic Engineering, University of Rajshahi, Rajshahi 6205, Bangladesh

<sup>b</sup> Department of Electrical and Electronic Engineering, North Bengal International University, Rajshahi 6100, Bangladesh

<sup>c</sup> Department of Electrical and Electronic Engineering, Begum Rokeya University, Rangpur, 5400, Bangladesh

## ARTICLE INFO

### Keywords:

Solar cell

Hole transport layer

TCO

SCAPS-1D

## ABSTRACT

Simulation of cadmium sulfide (CdS) and cadmium telluride (CdTe) based solar cell (ZnO/CdS/CdTe/NiO/Au) using Solar Cell Capacitance Simulator-1D (SCAPS-1D) has been presented in this article. Nickel oxide (NiO) and zinc oxide (ZnO) layers have been introduced as hole transport layer (HTL) and transparent conductive oxide (TCO), respectively. ZnO, CdS, and CdTe were synthesized using the facile chemical route, and their absorption coefficient was determined systematically. Later these experimentally found absorption coefficient data were used to study the effect of NiO HTL and ZnO TCO on the performance of CdS/CdTe based solar cell using SCAPS-1D. The impact of thickness, carrier concentration, defect density of the CdTe, and CdS/CdTe interface defect density on the solar cell performance was also investigated. The optimized solar cell demonstrated a maximum power conversion efficiency (PCE) of 28.04 % with open circuit voltage ( $V_{OC}$ ) of 1.09 V, short circuit current density ( $J_{SC}$ ) of 29.09 mA/cm<sup>2</sup> and FF of 87.84 % that shows huge promise in low-cost solar energy harvesting.

## 1. Introduction

Today, global energy demand is growing tremendously due to the increase of population, industrialization, and the widespread use of digital materials in almost every part of our daily lives. Fossil fuels are the primary source of energy [1]. A large amount of carbon dioxide (CO<sub>2</sub>) gas produces due to the combustion of fossil fuels [2]. Besides, this is not a sustainable source of energy. The energy sector is extending for these reasons, but moving to green renewable energy sources is the best solution. Solar cells could be a suitable alternative to fossil fuels. The highly efficient solar cells are silicon-based fabricated using very sophisticated and costly techniques [3]. The inexpensive third-generation thin-film solar cell is considered as a potential alternative of the single-crystal silicon (Si) solar cell [3]. Recently, many researchers have focused their attention on highly efficient perovskite and polymer solar cells [4,5]. Nevertheless, perovskite and polymer solar cells suffer from the problem of instability that restricts their long-term applications [6]. Therefore, ambient stable inorganic thin-film heterojunction solar cells can be a suitable alternative of perovskite and polymer solar cells [7,8].

The group III-V compounds and alloys, the chalcopyrite compound, copper indium gallium diselenide (CIGS), cadmium sulfide (CdS), cadmium selenide (CdSe) and cadmium telluride (CdTe) are the prime materials to be used in complete inorganic thin-film heterojunction solar cells [8]. The cadmium telluride (CdTe), copper indium gallium selenide (CIGS), and amorphous silicon (a-Si)

\* Corresponding author.

E-mail address: [ismail@ru.ac.bd](mailto:ismail@ru.ac.bd) (A.B.Md. Ismail).

based solar cells are the most successful thin-film solar cell [9]. The cost of CdTe technology is 40% lower than that of a-Si and 30 % lower than that of a-Si and 30 % lower than CIGS [10]. Therefore, with CdTe-based thin-film solar cells, the maximum ratio, "efficiency/cost" could be obtained. A laboratory CdS/CdTe solar cell has reported a high efficiency of 22.1 % [11].

CdTe is a p-type semiconducting material with a direct band gap of  $\sim 1.49$  eV, which very closely fits the solar spectrum [12]. The absorption coefficient of the CdTe is very high ( $\sim 10^5$  cm $^{-1}$ ) and can absorb more than 99 % of photons (with energy above the band gap) over several micrometers [13]. In coupled with CdTe, CdS forms a robust heterostructure. It is an n-type semiconductor with a direct wide band gap of 2.4 eV, can be used as a window layer in CdTe based solar cells [14]. The cell performance is greatly dependent on the energy barrier at the interface of absorber and back contact. The use of a low resistive back contact buffer layer with a high work function (WF) can reduce this energy barrier [15]. Recently, many researchers have worked on the back contact buffer layer for the CdTe based solar cells [15–18]. The high WF transition metal oxides (TMOs) like NiO [19], MoO<sub>x</sub> [17,20–22], WO<sub>3</sub> [23], V<sub>2</sub>O<sub>5</sub> [24,25] were introduced in many practical CdTe based solar cells as HTL (back contact buffer layer) for the performance enhancement; found very encouraging results. Among all TMOs, NiO is very promising HTL due to its high work function of  $\sim 5.0$  eV with a wide band gap of 3.5–3.8 eV [26–28]. It can be synthesized using a very low-cost solution process [29,30]. An optically transparent electrode is used at the front side of the solar cell to transport the photogenerated electrons to the external load. Generally, indium tin oxide (ITO) or fluorine-doped tin oxide (FTO) is used as TCO in the solar cell. The ITO and FTO are very expensive, and ITO suffers from instability issues [31,32]. ZnO can be used as TCO as an alternative of FTO and ITO due to its wide band gap (3.37 eV), excellent optical and electrical characteristics, and abundance in earth crust [33–35].

In addition, the different physical parameters like carrier concentration, thickness, and deep level defects of the absorber layer, window layer, and HTL have a significant role on the solar cell performance [28,36–39]. The thickness of the absorber layer higher than the carrier diffusion length could increase the recombination rate [40], and inadequate thickness intensifies the loss of photocurrent density [41]. Besides, the open circuit voltage of the solar cell could be enhanced with a suitable carrier concentration of the absorber layer [36]. The efficient transportation of electrons through the window layer and holes through the HTL depends on the suitable band alignment of these layers with the absorber layer [28]. The band alignment of the window layer and HTL with the absorber layer can be controlled by the doping concentration [42]. In a practical solar cell, the non-radiative recombination increases due to the increase of deep level defects in the absorber layer [37]. Therefore, the mentioned physical parameters have to be optimized for the development of high performance solar cells.

In this research, a novel heterostructure (ZnO/CdS/CdTe/NiO/Au) of highly efficient CdS/CdTe based solar cells has been designed. The numerical analysis of the designed solar cell has been conducted using SCAPS-1D computer simulation software. To achieve optimum solar cell performance, the effect of different physical parameters of the ZnO, CdTe, and NiO have investigated. The maximum efficiency of  $\sim 28$  % was recorded from the optimized solar cell.

## 2. Modeling and numerical simulation

Solar cell simulation software is made to solve the characteristics equations of semiconducting materials. AMPS-1D, SILVACO ATLAS, wxAMPS, COMSOL, and SCAPS-1D are the well-known solar cell simulator. SCAPS-1D is more popular than other simulators because of its ability to model a maximum seven-layer structure and non-routine measurements [43,44].

In this research, SCAPS-1D was used for the modeling and numerical simulation of the ZnO/CdS/CdTe/NiO/Au heterojunction solar cell. The J–V, C–V, C–f characteristics and quantum efficiency of the solar cell can be measured using the SCAPS-1D. It computes these numerical measurements of the modeled solar cell using the following equations (Eq. (1), (2), and (3)).

$$(Poisson's\ equation)\ \frac{\partial^2\Psi}{\partial x^2} + \frac{q}{\epsilon} \left[ p(x) - n(x) + N_D - N_A + \rho_p - \rho_n \right] = 0 \quad (1)$$

$$(Hole\ continuity\ equation)\ \frac{1}{q} \frac{\partial J_p}{\partial x} = G_{op} - R(x) \quad (2)$$

$$(Electron\ continuity\ equation)\ \frac{1}{q} \frac{\partial J_n}{\partial x} = -G_{op} + R(x) \quad (3)$$

Where  $\epsilon$  is the dielectric constant, q is the electron charge, N<sub>A</sub> and N<sub>D</sub> are ionized acceptors and donor density,  $\Psi$  is the electrostatic potential, J<sub>p</sub> is current density due to hole, J<sub>n</sub> is current density due to electron, G<sub>op</sub> is the carrier generation rate, R is the total recombination rate, p is free hole density, n is the free electron density, ρ<sub>p</sub> and ρ<sub>n</sub> are the hole and electron distribution.

The following drift-diffusion equations (Eq. (4) and (5)) represent the holes and electrons carrier transport properties of the semiconducting material.

$$J_p = -\frac{\mu_p p}{q} \frac{\partial E_{Fp}}{\partial x} \quad (4)$$

$$J_n = -\frac{\mu_n n}{q} \frac{\partial E_{Fn}}{\partial x} \quad (5)$$

Where  $\mu_p$  and  $\mu_n$  are the hole and electron mobility, E<sub>Fp</sub> and E<sub>Fn</sub> are the p-type and n-type carrier fermi level.

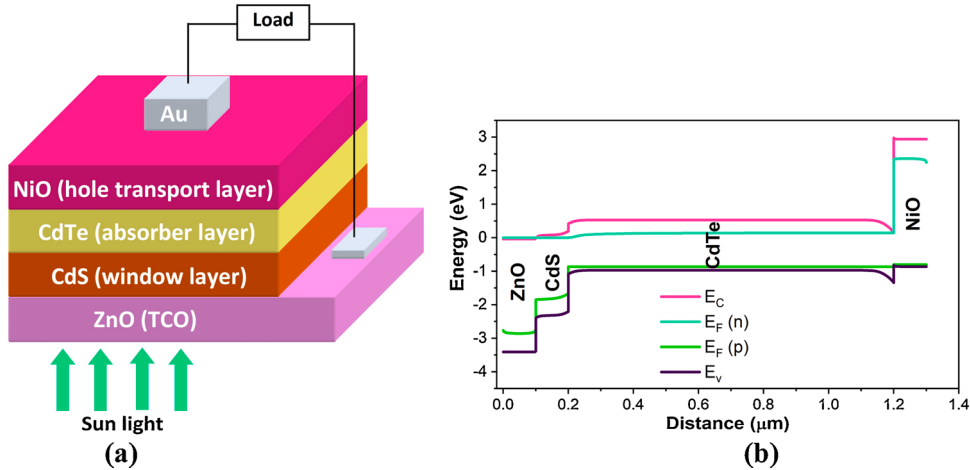


**Fig. 1.** (a) Schematic diagram, and (b) energy band diagram of the ZnO/CdS/CdTe/ NiO heterojunction solar cell.

**Table 1**

Default parameters of the FTO [25], ZnO [50], CdS [25,51], CdTe [25] and NiO [28,52] for the simulation of ZnO/CdS/CdTe/NiO/Au solar cell.

Parameters	FTO	ZnO	CdS	CdTe	NiO
Thickness (nm)	300	100	100	1000	100
Bandgap (eV)	3.5	3.37	2.4	1.5	3.8
Electron affinity (eV)	4.5	4.5	4.5	4.28	1.46
Dielectric permittivity (relative)	10	9	10	10.3	10
CB effective density of states ( $\text{cm}^{-3}$ )	$2 \times 10^{18}$	$2.2 \times 10^{18}$	$2.2 \times 10^{18}$	$9.2 \times 10^{17}$	$2.8 \times 10^{19}$
VB effective density of states ( $\text{cm}^{-3}$ )	$1.8 \times 10^{19}$	$1.8 \times 10^{19}$	$1.9 \times 10^{19}$	$5.2 \times 10^{18}$	$1 \times 10^{19}$
Electron mobility ( $\text{cm}^2/\text{Vs}$ )	100	100	350	320	12
Hole mobility ( $\text{cm}^2/\text{Vs}$ )	20	25	25	40	2.8
Shallow uniform donor density $N_D$ ( $\text{cm}^{-3}$ )	$10^{17}$	$10^{19}$	$10^{27}$	0	0
Shallow uniform acceptor density $N_A$ ( $\text{cm}^{-3}$ )	0	0	0	$10^{17}$	$10^{18}$
Electron thermal velocity ( $\text{cm}/\text{s}$ )	$10^7$	$10^7$	$10^7$	$10^7$	$10^7$
Hole thermal velocity ( $\text{cm}/\text{s}$ )	$10^7$	$10^7$	$10^7$	$10^7$	$10^7$
Defect density ( $\text{cm}^{-3}$ )	0	$10^{14}$	$10^{14}$	$10^{14}$	$10^{14}$
Radiative recombination coefficient ( $\text{cm}^3/\text{s}$ )	0	$2.3 \times 10^{-9}$	$2.3 \times 10^{-9}$	$2.3 \times 10^{-9}$	$2.3 \times 10^{-9}$

**Table 2**  
Interface parameters.

Parameters	CdS/CdTe interface
Defect type	Neutral
Capture cross section electrons ( $\text{cm}^2$ )	$1 \times 10^{-19}$
Capture cross-section holes ( $\text{cm}^2$ )	$1 \times 10^{-19}$
Reference for defect energy level $E_t$	above the highest $E_v$
The energy with respect to Reference (eV)	0.06
Total density (integrated over all energies) ( $1/\text{cm}^2$ )	$1 \times 10^{10}$

### 3. Solar cell structure and materials properties

Fig. 1(a,b) shows the schematic and energy band diagram of the ZnO/CdS/CdTe/NiO/Au solar cell where ZnO, CdS, CdTe, NiO, and Au were used as TCO, window layer, absorber layer, HTL, and back metal contact respectively. ZnO is an n-type semiconductor with a broad band gap of 3.37 eV; provides outstanding features like high transparency, and excellent electrical properties; a promising TCO as an alternative of FTO and ITO for the thin-film solar cells [45–47]. From our experimental study, the band gap of ZnO, CdS, CdTe were found 3.37, 2.4, and 1.5 eV, respectively. The experimental optical properties of CdS and CdTe were described in our previous reports [48,49]. The default physical parameters of the ZnO, CdS, CdTe, and NiO used for the numerical simulation are listed in Table 1 and Table 2.

### 4. Results and discussion

The J-V characteristic and quantum efficiency (QE) of the ZnO/CdS/CdTe/Au, FTO/CdS/CdTe/NiO/Au and ZnO/CdS/CdTe/NiO/

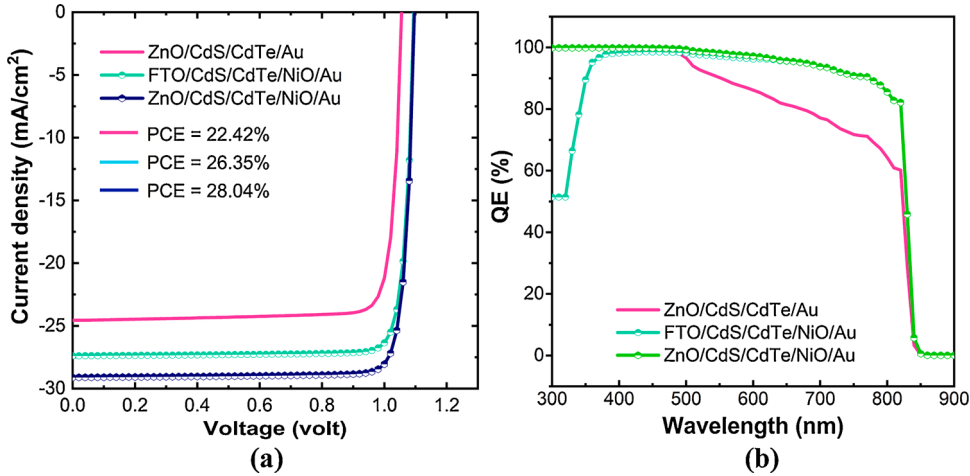


**Fig. 2.** (a) The J-V characteristic and (b) quantum efficiency (QE) of the ZnO/CdS/CdTe/Au, FTO/CdS/CdTe/NiO/Au, ZnO/CdS/CdTe/NiO/Au solar cell.

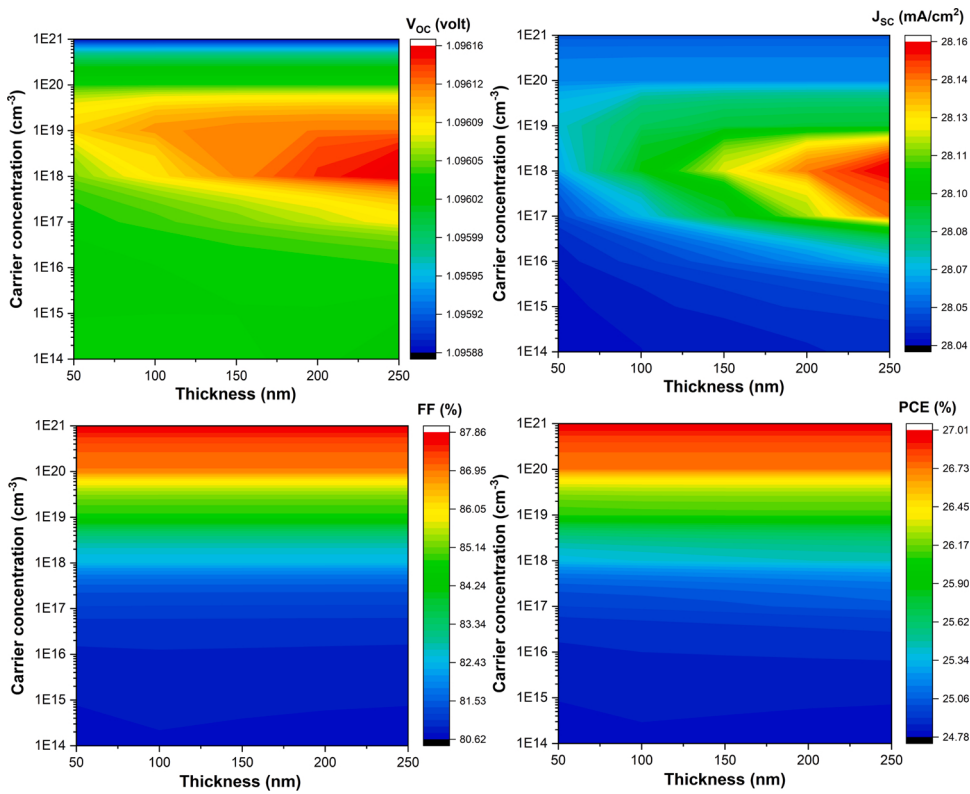


**Fig. 3.** The dependency of the cell performance on the carrier concentration and thickness of the NiO HTL.

Au solar cell are depicted in Fig. 2. The  $V_{\text{OC}}$ ,  $J_{\text{SC}}$ , FF and PCE of 1.09 V,  $29.09 \text{ mA}/\text{cm}^2$ , 87.84 % and 28.04 % respectively achieved from the optimized ZnO/CdS/CdTe/NiO/Au solar cell where FTO/CdS/CdTe/NiO/Au solar cell produced  $V_{\text{OC}}$  of 1.09 V,  $J_{\text{SC}}$  27.38  $\text{mA}/\text{cm}^2$ , FF 87.85 % and PCE 26.35 %; and ZnO/CdS/CdTe/Au solar cell produced  $V_{\text{OC}}$  of 1.06 V,  $J_{\text{SC}}$  24.56  $\text{mA}/\text{cm}^2$ , FF 86.46 % and PCE 22.42 %. Huge performance enhancement is observed from Fig. 2 after incorporation of the NiO as HTL in CdS/CdTe based solar cell with ZnO as TCO. It is observed from Fig. 2(b) that quantum efficiency of the cell improved between 500–800 nm of wavelength after incorporation of NiO HTL and this improvement of QE indicates the reduction of surface carrier recombination at CdTe, which revealed the enhancement of PCE after using NiO HTL. ZnO TCO alternative of FTO improved the quantum efficiency below 400 nm of

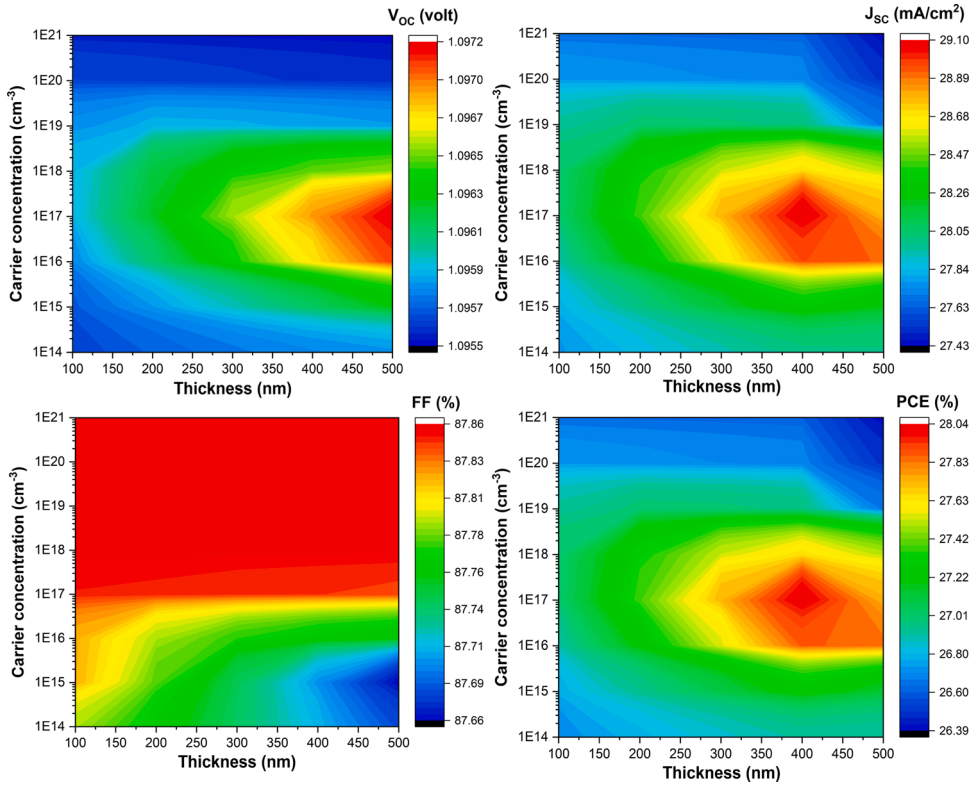


**Fig. 4.** The cell performance dependency on the carrier concentration and thickness of the ZnO TCO.

wavelength, supports the results of PCE.

#### 4.1. Influence of carrier concentration and thickness of the NiO HTL

Fig. 3 shows the cell performance with respect to the carrier concentration and thickness of the NiO HTL. It is seen from Fig. 3 that the  $V_{OC}$  is almost independent with the carrier concentration and thickness of the NiO HTL. The  $J_{SC}$  changes slightly with the carrier concentration and thickness. The optimum  $J_{SC}$  of  $28.16 \text{ mA}/\text{cm}^2$  was produced at NiO carrier concentration of  $10^{18} \text{ cm}^{-3}$  and thickness of 250 nm. The FF was found increasing with increasing the carrier concentration but almost unchanged with thickness. The decrease of series resistance with increasing carrier concentration is the reason for the increase of FF [28]. The PCE showed the same trend as FF. The maximum PCE of 27.01 % was obtained at a carrier concentration of  $10^{21} \text{ cm}^{-3}$ .

#### 4.2. Influence of carrier concentration and thickness of the ZnO TCO

The dependency of the cell performance on the carrier concentration and thickness of the ZnO TCO is depicted in Fig. 4. It is observed from Fig. 4 that ZnO thickness has no influence on the  $V_{OC}$  but changes with the carrier concentration and found the optimum value of  $1.0972 \text{ V}$  at  $10^{17} \text{ cm}^{-3}$ . The  $J_{SC}$  exhibited the same nature of  $V_{OC}$  and produced optimum  $J_{SC}$  of  $29.1 \text{ mA}/\text{cm}^2$  at carrier concentration of  $10^{17} \text{ cm}^{-3}$ . The increase of carrier concentration of ZnO promoted the band bending, which resulted in a slight increase of  $J_{SC}$  [53]. The FF showed decreasing nature with the thickness of ZnO till carrier concentration of  $10^{17} \text{ cm}^{-3}$  due to the increase of series resistance of the cell [54]. The cell with carrier concentration and thickness of  $10^{17} \text{ cm}^{-3}$  and 400 nm exhibited a maximum PCE of 28.04 %.

#### 4.3. Influence of carrier concentration and thickness of the CdTe absorber layer

The variation of cell performance with the carrier concentration and thickness of the CdTe absorber layer is depicted in Fig. 5. The increase of CdTe carrier concentration results in the increase of band bending at CdTe, which promotes the built-in potential at the CdS/CdTe p-n junction and reduces the recombination rate at the interface [55]. The highest  $V_{OC}$  of  $1.143 \text{ V}$  was obtained at carrier concentration of  $10^{20} \text{ cm}^{-3}$  and thickness of 200 nm. At the carrier concentration  $<10^{19} \text{ cm}^{-3}$ , the  $V_{OC}$  increases with carrier concentration and decreases with the thickness of the CdTe absorber layer.  $V_{OC}$  is independent of the CdTe absorber layer thickness at carrier concentration of  $>10^{19} \text{ cm}^{-3}$ .  $J_{SC}$  shows the reverse trend of  $V_{OC}$  and optimum  $29.10 \text{ mA}/\text{cm}^2$   $J_{SC}$  obtained at carrier

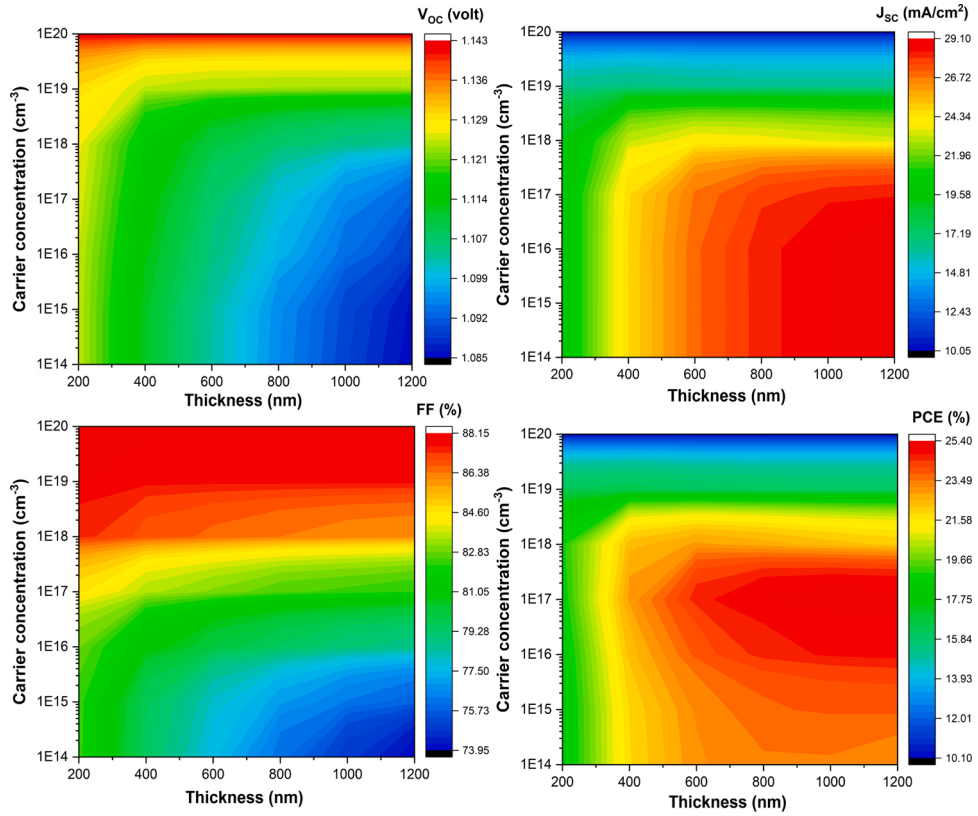


**Fig. 5.** The cell performance dependency on the carrier concentration and thickness of the CdTe absorber layer.

concentration and thickness of  $10^{16} \text{ cm}^{-3}$  and 1000 nm, respectively. With increasing CdTe carrier concentration, the series resistance was decreased, which was reflected in the FF [56]. The highest FF of 88.15 % was achieved at carrier concentration  $>10^{18} \text{ cm}^{-3}$  and thickness  $>800 \text{ nm}$ . The maximum PCE of 25.4 % was shown at carrier concentration of  $10^{17} \text{ cm}^{-3}$  and thickness of 1000 nm.

#### 4.4. Effect of the defect density and thickness of the CdTe absorber layer

The response of cell performance with defect density and thickness of the CdTe absorber layer is shown in Fig. 6. The decrease of  $V_{\text{OC}}$  is observed with increasing defect density and thickness, where no influence of defect density on  $J_{\text{SC}}$  is observed below the defect density of  $10^{15} \text{ cm}^{-3}$ . At the defect density of  $10^{14} \text{ cm}^{-3}$  and thickness of 1200 nm, optimum  $28.25 \text{ mA/cm}^2 J_{\text{SC}}$  was achieved. FF is correlated with  $V_{\text{OC}}$  and carrier recombination process [57], shows the same trend of  $V_{\text{OC}}$ . The PCE is proportionally related to  $V_{\text{OC}}$ ,  $J_{\text{SC}}$ , and FF. A maximum PCE of 25.41 % was observed at defect density of  $10^{11} \text{ cm}^{-3}$  and thickness of 1000 nm.

#### 4.5. Effect of the CdS/CdTe interface defect density

Fig. 7 depicts the effect of the CdS/CdTe interface defect density and thickness of the CdTe absorber layer on the cell performance. It is observed from Fig. 7 that absorber layer thickness has no impact on  $V_{\text{OC}}$  but decreases with the interface defect density. The interface defect density does not influence the  $J_{\text{SC}}$  till  $<10^{17} \text{ cm}^{-2}$ , while the  $J_{\text{SC}}$  increases from 19.58 to  $28.23 \text{ mA/cm}^2$  for absorber thickness from 200 to 1200 nm. The FF reduces drastically from 83.8–53.8% for the increase of interface defect density from  $10^{11}$  to  $10^{18} \text{ cm}^{-2}$ . A massive decrement of PCE from 25.3–4.3% also observed with the interface defect density from  $10^{11}$  to  $10^{18} \text{ cm}^{-2}$ . Interface defect is one of the significant contributing agents to the series resistance [58], responsible for the low PCE. Interfacial defect density induces in the cell due to the production of structural defects of the materials during the fabrication process.

#### 4.6. Influence of CdTe electron affinity and back contact metal work function

The influence of electron affinity (EA) of the CdTe absorber layer is illustrated in Fig. 8(a). The optimum cell performance was observed at CdTe EA of 4.17 eV. As shown in Fig. 8(a), the PCE decreases with EA  $> 4.17 \text{ eV}$  due to the decrease of FF [59]. The effect of back contact metal work function (WF) is depicted in Fig. 8(b). It is observed that the  $V_{\text{OC}}$  increases with metal WF. Therefore, PCE

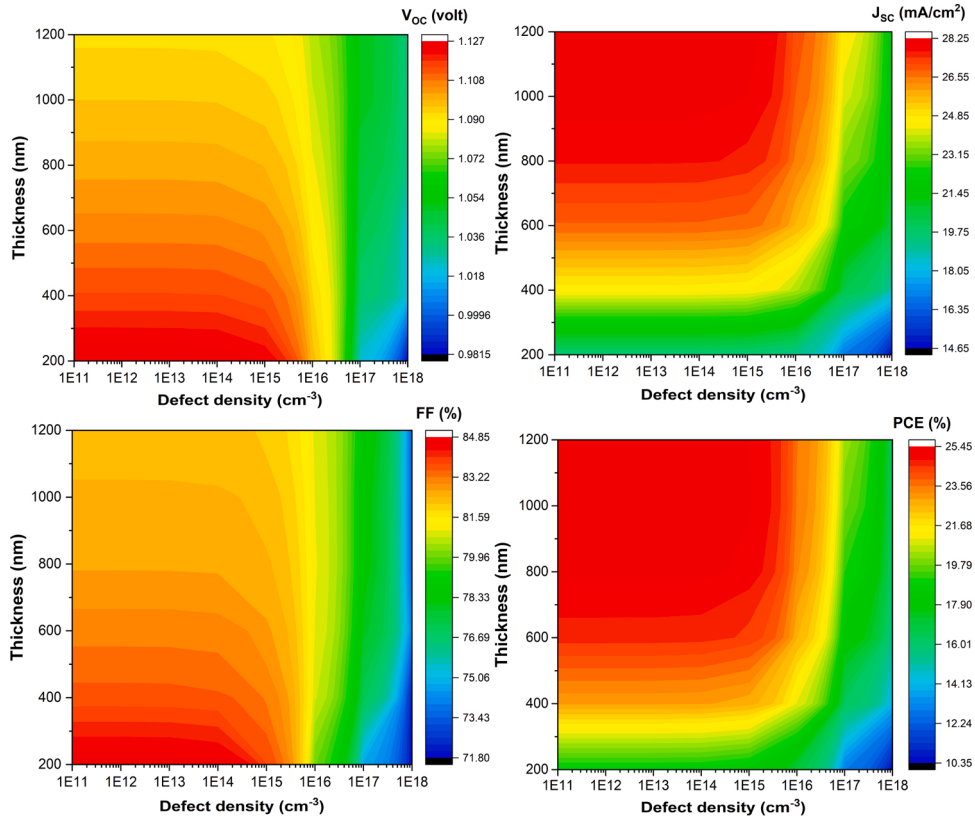


**Fig. 6.** Effect of the defect density and thickness of the CdTe absorber layer on the cell performance.

increases with metal WF till 4.9 eV. The PCE saturated after WF of 4.9 eV. The energy barrier of the majority carrier at the metal-semiconductor interface decreases with increasing the metal WF, which is beneficial to make suitable ohmic contact [60]. Therefore, it is crucial to select an appropriate metal contact to optimize the cell performance.

## 5. Conclusion

We have demonstrated that NiO is a promising hole transport material that offers the potential for further efficiency enhancement of the CdS/CdTe-based solar cells. ZnO TCO could be a suitable alternative of ITO and FTO for the development of low-cost, highly efficient CdS/CdTe-based solar cells. The maximum PCE of 28.04 % was obtained at NiO and ZnO carrier concentration of  $10^{21} \text{ cm}^{-3}$  and  $10^{17} \text{ cm}^{-3}$ , respectively, and thickness of 100 nm and 400 nm, respectively. The carrier concentration, thickness, and deep level defect density of the CdTe absorber layer were also studied. The PCE was found to increase with absorber layer thickness. The maximum PCE was obtained at carrier concentration and thickness of  $10^{17} \text{ cm}^{-3}$  and 1000 nm, respectively. CdTe defect density and CdS/CdTe interface defect density were also optimized. The solar cell with CdTe defect density of  $<10^{14} \text{ cm}^{-3}$  and CdS/CdTe interface defect density of  $<10^{12} \text{ cm}^{-2}$  shown the best performance. Therefore, this study could provide the necessary protocols for the practical design and optimization of the high performance CdS/CdTe based solar cells with NiO HTL and ZnO TCO layer.

## Declaration of Competing Interest

The authors report no declarations of interest.

## Acknowledgements

The authors gratefully acknowledge Dr. Marc Burgelman, University of Gent, Belgium, for providing SCAPS 1-D simulation software.

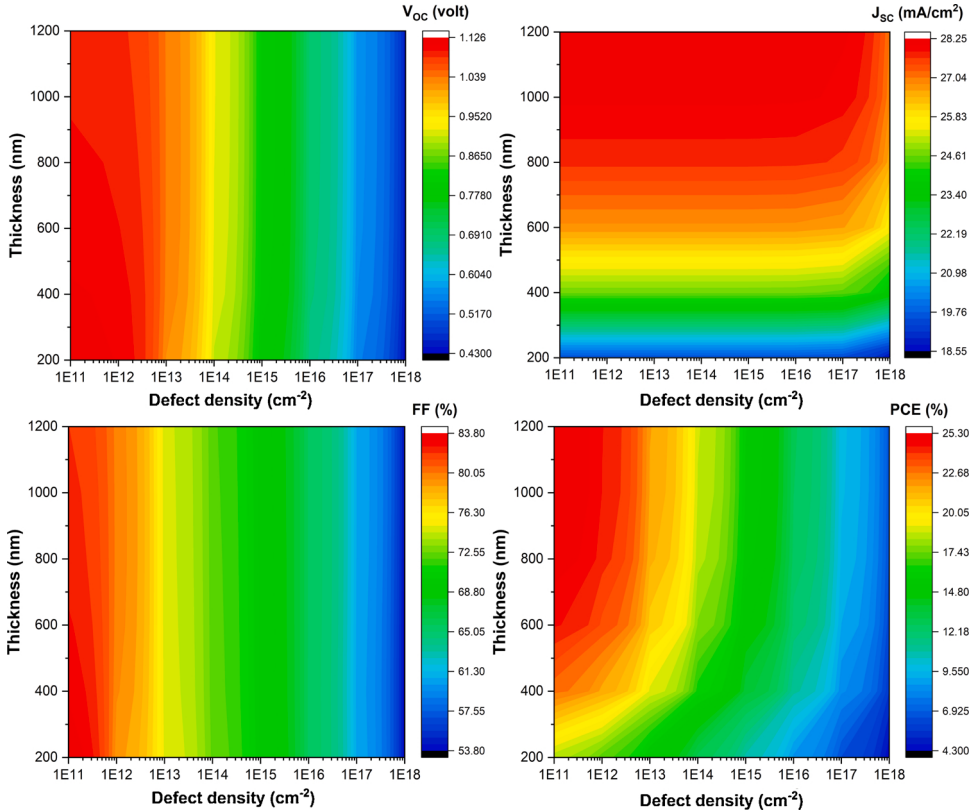


**Fig. 7.** Effect of the CdS/CdTe interface defect density and thickness of the CdTe absorber layer on the cell performance.

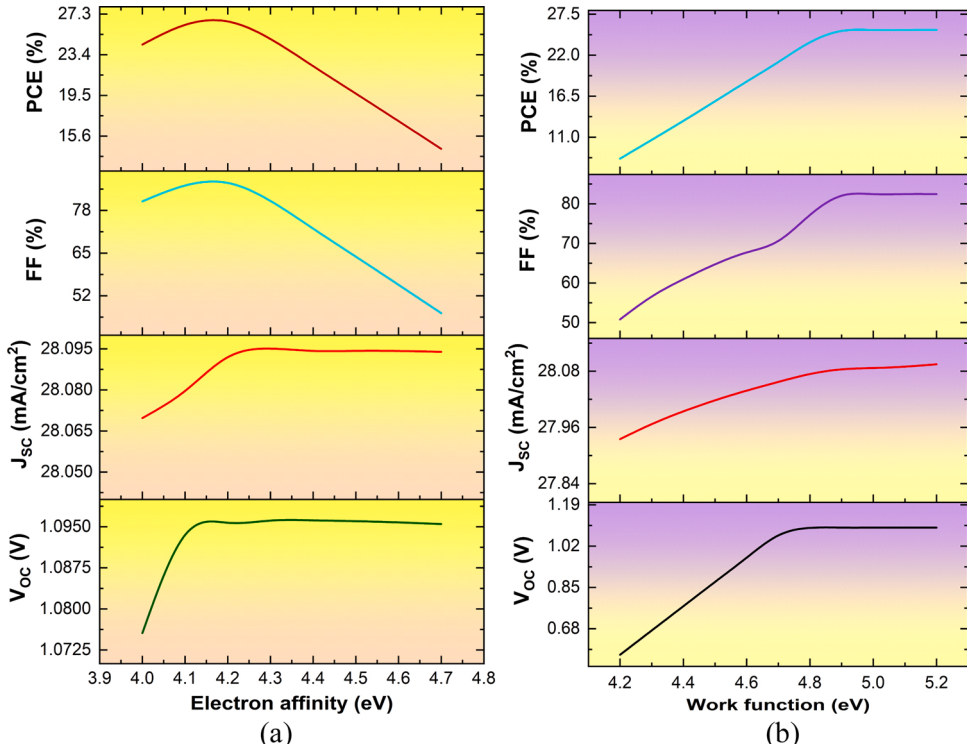


**Fig. 8.** Cell performance parameters as a function of CdTe (a) electron affinity and (b) work function of back contact metal.

## References

- [1] B. Sundén, Introduction and background. *Hydrog. Batter. Fuel Cells*, Elsevier, 2019, pp. 1–13.
- [2] G.P. Hammond, P.J.G. Pearson, Challenges of the transition to a low carbon, more electric future: from here to 2050, *Energy Policy* 52 (2013) 1–9.
- [3] K.-S. Liao, S.D. Yambem, A. Haldar, N.J. Alley, S.A. Curran, Designs and architectures for the next generation of organic solar cells, *Energies* 3 (2010) 1212–1250.
- [4] J. Huang, S. Xiang, J. Yu, C.-Z. Li, Highly efficient prismatic perovskite solar cells, *Energy Environ. Sci.* 12 (2019) 929–937.
- [5] Y. Wang, Q. Fan, X. Guo, W. Li, B. Guo, W. Su, X. Ou, M. Zhang, High-performance nonfullerene polymer solar cells based on a fluorinated wide bandgap copolymer with a high open-circuit voltage of 1.04 V, *J. Mater. Chem. A* 5 (2017) 22180–22185.
- [6] Z. Yi, N.H. Ladi, X. Shai, H. Li, Y. Shen, M. Wang, Will organic–inorganic hybrid halide lead perovskites be eliminated from optoelectronic applications? *Nanoscale Adv.* 1 (2019) 1276–1289.
- [7] T.K. Townsend, E.E. Foos, Fully solution processed all inorganic nanocrystal solar cells, *Phys. Chem. Chem. Phys.* 16 (2014) 16458–16464.
- [8] R.W. Miles, G. Zoppi, I. Forbes, Inorganic photovoltaic cells, *Mater. Today* 10 (2007) 20–27.
- [9] M.A. Green, K. Emery, Y. Hishikawa, W. Warta, Solar cell efficiency tables (version 37), *Prog. Photovoltaics Res. Appl.* 19 (2011) 84–92.
- [10] R. Swami, Solar cell, *Int. J. Sci. Res. Publ.* 2 (2012) 1–5.
- [11] L.I. Nykyryu, R.S. Yavorskyi, Z.R. Zapukhlyak, G. Wisz, P. Potera, Evaluation of CdS/CdTe thin film solar cells: SCAPS thickness simulation and analysis of optical properties, *Opt. Mater. (Amst.)* 92 (2019) 319–329.
- [12] S. Du, L. Zhu, W. Li, J. Zhang, L. Wu, W. Wang, Bilayered ZnTe/Cu<sub>1.4</sub>Te alloy thin films as a back contact for CdTe solar cells, *Sol. Energy* 185 (2019) 262–269.
- [13] F. He, X. Yin, J. Li, S. Lin, L. Wu, X. Hao, J. Zhang, L. Feng, Characterization of sputtered MoO<sub>x</sub> thin films with different oxygen content and their application as back contact in CdTe solar cells, *Vacuum* 176 (2020) 109337.
- [14] J. Qi, W. Liu, C. Biswas, G. Zhang, L. Sun, Z. Wang, X. Hu, Y. Zhang, Enhanced power conversion efficiency of CdS quantum dot sensitized solar cells with ZnO nanowire arrays as the photoanodes, *Opt. Commun.* 349 (2015) 198–202.
- [15] J. Liu, X. Liu, K. Yang, S. He, H. Lu, B. Li, G. Zeng, J. Zhang, W. Li, L. Wu, L. Feng, Preparation and characterization of pulsed laser deposited Sb<sub>2</sub>Te<sub>3</sub> back contact for CdTe thin film solar cell, *Appl. Surf. Sci.* 453 (2018) 126–131.
- [16] S.H. Demtsu, J.R. Sites, Effect of back-contact barrier on thin-film CdTe solar cells, *Thin Solid Films* 510 (2006) 320–324.
- [17] R. Yang, D. Wang, M. Jeng, K. Ho, D. Wang, Stable CdTe thin film solar cells with a MoO<sub>x</sub> back-contact buffer layer, *Prog. Photovoltaics Res. Appl.* 24 (2016) 59–65.
- [18] A.L. Fahrnenbruch, Exploring back contact technology to increase CdS/CdTe solar cell efficiency, *MRS Proc.* 1012 (2007), 1012-Y07-05.
- [19] X. Di Xiao, D. Li, Q. Wang, K. Li, D. Shen, Wang, CdTe thin film solar cell with NiO as a back contact buffer layer, *Sol. Energy Mater. Sol. Cells* 169 (2017) 61–67.
- [20] I. Irfan, H. Lin, W. Xia, H.N. Wu, C.W. Tang, Y. Gao, The effect of MoO<sub>x</sub> inter-layer on thin film CdTe/CdS solar cell, *Sol. Energy Mater. Sol. Cells* 105 (2012) 86–89.
- [21] H. Lin, Irfan, W. Xia, H.N. Wu, Y. Gao, MoO<sub>x</sub>back contact for CdS/CdTe thin film solar cells: Preparation, device characteristics, and stability, *Sol. Energy Mater. Sol. Cells* 99 (2012) 349–355.
- [22] N.R. Paudel, A.D. Compaan, Y. Yan, Sputtered CdS/CdTe solar cells with MoO<sub>3-x</sub>/Au back contacts, *Sol. Energy Mater. Sol. Cells* 113 (2013) 26–30.
- [23] N.R. Paudel, C. Xiao, Y. Yan, CdS/CdTe thin-film solar cells with Cu-free transition metal oxide/Au back contacts, *Prog. Photovoltaics Res. Appl.* 23 (2015) 437–442.
- [24] K. Shen, R. Yang, D. Wang, M. Jeng, S. Chaudhary, K. Ho, D. Wang, Stable CdTe solar cell with V<sub>2</sub>O<sub>5</sub> as a back contact buffer layer, *Sol. Energy Mater. Sol. Cells* 144 (2016) 500–508.
- [25] A. Kuddus, M.F. Rahman, S. Ahmed, J. Hossain, A.B.M. Ismail, Role of facile synthesized V<sub>2</sub>O<sub>5</sub> as hole transport layer for CdS/CdTe heterojunction solar cell: validation of simulation using experimental data, *Superlattices Microstruct.* 132 (2019), 106168.
- [26] K.-C. Wang, J.-Y. Jeng, P.-S. Shen, Y.-C. Chang, E.W.-G. Diau, C.-H. Tsai, T.-Y. Chao, H.-C. Hsu, P.-Y. Lin, P. Chen, T.-F. Guo, T.-C. Wen, P-type mesoscopic nickel oxide/organometallic perovskite heterojunction solar cells, *Sci. Rep.* 4 (2015) 4756.
- [27] I.-M. Chan, T.-Y. Hsu, F.C. Hong, Enhanced hole injections in organic light-emitting devices by depositing nickel oxide on indium tin oxide anode, *Appl. Phys. Lett.* 81 (2002) 1899–1901.
- [28] S. Ahmed, A. Aktar, J. Hossain, A.B.M. Ismail, Enhancing the open circuit voltage of the SnS based heterojunction solar cell using NiO HTL, *Sol. Energy* 207 (2020) 693–702.
- [29] Q. He, K. Yao, X. Wang, X. Xia, S. Leng, F. Li, Room-temperature and solution-processable Cu-doped nickel oxide nanoparticles for efficient hole-transport layers of flexible large-area perovskite solar cells, *ACS Appl. Mater. Interfaces* 9 (2017) 41887–41897.
- [30] J.W. Jung, C.-C. Chueh, A.K.Y. Jen, A. Low-Temperature, Solution-processable, Cu-doped nickel oxide hole-transporting layer via the combustion method for high-performance thin-film perovskite solar cells, *Adv. Mater.* 27 (2015) 7874–7880.
- [31] A. Way, J. Luke, A.D. Evans, Z. Li, J.S. Kim, J.R. Durrant, H.K. Hin Lee, W.C. Tsoi, Fluorine doped tin oxide as an alternative of indium tin oxide for bottom electrode of semi-transparent organic photovoltaic devices, *AIP Adv.* 9 (2019).
- [32] H.-Y. Yang, W.-J. Ho, S.-K. Feng, J.-J. Liu, T.-W. Chuang, G.-Y. Li, Y.-C. Yang, C.-C. Chiang, Y.-H. Chen, Electrical and optical performance of silicon solar cells using plasmonics indium nanoparticles layer embedded in SiO<sub>2</sub> antireflective coating, 2017 IEEE 44th Photovolt. Spec. Conf., IEEE (2017) 2664–2666.
- [33] S. Agrawal, R. Rane, S. Mukherjee, ZnO thin film deposition for TCO application in solar cell, *Conf. Pap. Energy.* 2013 (2013) 1–7.
- [34] T.P. Rao, M.C.S. Kumar, S.A. Angayarkanni, M. Ashok, Effect of stress on optical band gap of ZnO thin films with substrate temperature by spray pyrolysis, *J. Alloys Compd.* 485 (2009) 413–417.
- [35] E. Muchuweni, T.S. Sathiaraj, H. Nyakotyo, Synthesis and characterization of zinc oxide thin films for optoelectronic applications, *Heliyon* 3 (2017) e00285.
- [36] A. Kanevec, M.O. Reese, T.M. Barnes, S.A. Jensen, W.K. Metzger, The roles of carrier concentration and interface, bulk, and grain-boundary recombination for 25% efficient CdTe solar cells, *J. Appl. Phys.* 121 (2017) 0–9.
- [37] P.K. Nayak, S. Mahesh, H.J. Snaith, D. Cahen, Photovoltaic solar cell technologies: analysing the state of the art, *Nat. Rev. Mater.* 4 (2019) 269–285.
- [38] N. Kavitha, R. Chandramohan, S. Valanarasu, T.A. Vijayan, S.R. Rosario, A. Kathalingam, Effect of film thickness on the solar cell performance of CBD grown CdS/PbS heterostructure, *J. Mater. Sci. Mater. Electron.* 27 (2016) 2574–2580.
- [39] M.A. Rehman, S.B. Roy, I. Akhtar, M.F. Bhopal, W. Choi, G. Nazir, M.F. Khan, S. Kumar, J. Eom, S.H. Chun, Y. Seo, Thickness-dependent efficiency of directly grown graphene based solar cells, *Carbon N. Y.* 148 (2019) 187–195.
- [40] V. Manjunath, R. Krishna, S. Maniarasu, E. Ramasamy, S. Shanmugasundaram, G. Veerappan, Perovskite solar cell architectures. *Perovskite Photovoltaics*, Elsevier, 2018, pp. 89–121.
- [41] L.A. Kosyachenko, Possibilities to decrease the absorber thickness reducing optical and recombination losses in CdS/CdTe solar cells, *Mater. Renew. Sustain. Energy* 2 (2013) 1–20.
- [42] A. Kaphle, E. Echeverria, D.N. McIlroy, P. Hari, Enhancement in the performance of nanostructured CuO–ZnO solar cells by band alignment, *RSC Adv.* 10 (2020) 7839–7854.
- [43] M.M.A. Moon, M.H. Ali, M.F. Rahman, J. Hossain, A.B.M. Ismail, Design and simulation of FeSi<sub>2</sub>-based novel heterojunction solar cells for harnessing visible and near-infrared light, *Phys. Status Solidi* 217 (2020), 1900921.
- [44] L. Et-taya, T. Ouslimane, A. Benami, Numerical analysis of earth-abundant Cu<sub>2</sub>ZnSn(S<sub>x</sub>Se<sub>1-x</sub>)<sub>4</sub> solar cells based on Spectroscopic Ellipsometry results by using SCAPS-1D, *Sol. Energy* 201 (2020) 827–835.
- [45] A.K. Ambedkar, M. Singh, V. Kumar, V. Kumar, B.P. Singh, A. Kumar, Y.K. Gautam, Structural, optical and thermoelectric properties of Al-doped ZnO thin films prepared by spray pyrolysis, *Surf. Interfaces* 19 (2020), 100504.
- [46] A. Hongsingthong, I. Afidi Yunaz, S. Miyajima, M. Konagai, Preparation of ZnO thin films using MOCVD technique with D<sub>2</sub>O/H<sub>2</sub>O gas mixture for use as TCO in silicon-based thin film solar cells, *Sol. Energy Mater. Sol. Cells*, Elsevier, 2011, pp. 171–174.

- [47] L. Meng, H. Chai, X. Yang, Z. Lv, T. Yang, Optically rough and physically flat TCO substrate formed by coating ZnO thin film on pyramid-patterned glass substrate, *Sol. Energy Mater. Sol. Cells* 191 (2019) 459–465.
- [48] M.F. Rahman, J. Hossain, A. Kuddus, M.M.A. Moon, A.B.M. Ismail, Effect of Triton X-100 surfactant on thiol-amine cosolvents assisted facile synthesized CdS thin films on glass substrate by spin coating method, *SN Appl. Sci.* 2 (2020) 590.
- [49] M.F. Rahman, J. Hossain, A. Kuddus, S. Tabassum, M.H.K. Rubel, M.M. Rahman, Y. Moriya, H. Shirai, A.B.M. Ismail, A novel CdTe ink-assisted direct synthesis of CdTe thin films for the solution-processed CdTe solar cells, *J. Mater. Sci.* 55 (2020) 7715–7730.
- [50] S. Boudour, I. Bouchama, M. Hadjeb, S. Laidoudi, Optimization of defected ZnO/Si/Cu<sub>2</sub>O heterostructure solar cell, *Opt. Mater. (Amst)* 98 (2019), 109433.
- [51] M.S. Chowdhury, S.A. Shahahmadi, P. Chelvanathan, S.K. Tiong, N. Amin, K. Techato, N. Nuthammanachot, T. Chowdhury, M. Suklueng, Effect of deep-level defect density of the absorber layer and n/i interface in perovskite solar cells by SCAPS-1D, *Results Phys.* 16 (2020), 102839.
- [52] M.I. Hossain, F.H. Alharbi, N. Tabet, Copper oxide as inorganic hole transport material for lead halide perovskite based solar cells, *Sol. Energy* 120 (2015) 370–380.
- [53] M. Yue, J. Su, P. Zhao, Z. Lin, J. Zhang, J. Chang, Y. Hao, Optimizing the performance of CsPbI<sub>3</sub>-based perovskite solar cells via doping a ZnO electron transport layer coupled with interface engineering, *Nano-Micro Lett.* 11 (2019) 91.
- [54] M.F. Mohamad Noh, C.H. Teh, R. Dailk, E.L. Lim, C.C. Yap, M.A. Ibrahim, N. Ahmad Ludin, A.R. Bin Mohd Yusoff, J. Jang, M.A. Mat Teridi, The architecture of the electron transport layer for a perovskite solar cell, *J. Mater. Chem. C* 6 (2018) 682–712.
- [55] G. Kartopu, O. Oklobia, D. Turkay, D.R. Diercks, B.P. Gorman, V. Barrioz, S. Campbell, J.D. Major, M.K. Al Turkestani, S. Yerci, T.M. Barnes, N.S. Beattie, G. Zoppi, S. Jones, S.J.C. Irvine, Study of thin film poly-crystalline CdTe solar cells presenting high acceptor concentrations achieved by in-situ arsenic doping, *Sol. Energy Mater. Sol. Cells* 194 (2019) 259–267.
- [56] M. Dadu, A. Kapoor, K.N. Tripathi, Effect of operating current dependent series resistance on the fill factor of a solar cell, *Sol. Energy Mater. Sol. Cells* 71 (2002) 213–218.
- [57] E.S. Hossain, P. Chelvanathan, S.A. Shahahmadi, K. Sopian, B. Bais, N. Amin, Performance assessment of Cu<sub>2</sub>SnS<sub>3</sub>(CTS) based thin film solar cells by AMPS-1D, *Curr. Appl. Phys.* 18 (2018) 79–89.
- [58] Z. Gu, F. Chen, X. Zhang, Y. Liu, C. Fan, G. Wu, H. Li, H. Chen, Novel planar heterostructure perovskite solar cells with CdS nanorods array as electron transport layer, *Sol. Energy Mater. Sol. Cells* 140 (2015) 396–404.
- [59] M. Asaduzzaman, M. Hasan, A.N. Bahar, An investigation into the effects of band gap and doping concentration on Cu(In,Ga)Se<sub>2</sub> solar cell efficiency, *Springerplus* 5 (2016) 578.
- [60] C. Aliani, M. Krichen, A. Zouari, Effect of the front-metal work function on the performance of a-Si:H(n+)/a-Si:H(i)/c-Si(p) heterojunction solar cells, *J. Comput. Electron.* 18 (2019) 576–583.